Journal of Nuclear Materials 404 (2010) 25–32

Contents lists available at ScienceDirect

Journal of Nuclear Materials

journal homepage: www.elsevier.com/locate/jnucmat

Modeled salt density for nuclear material estimation in the treatment of spent nuclear fuel

Robert D. Mariani, DeeEarl Vaden *

Idaho National Laboratory, Pyroprocessing Technology Department, P.O. Box 1625, Idaho Falls, ID 83415-6180, USA

ARTICLE INFO

Article history:
Received 10 December 2009
Accepted 14 June 2010

ABSTRACT

Spent metallic nuclear fuel is being treated in a pyrometallurgical process that includes electrorefining the uranium metal in molten eutectic LiCl–KCl as the supporting electrolyte. We report a model for determining the density of the molten salt. Material balances account for the net mass of salt and for the mass of actinides present. It was necessary to know the molten salt density, but difficult to measure. It was also decided to model the salt density for the initial treatment operations. The model assumes that volumes are additive for the ideal molten salt solution as a starting point; subsequently, a correction factor for the lanthanides and actinides was developed. After applying the correction factor, the percent difference between the net salt mass in the electrorefiner and the resulting modeled salt mass decreased from more than 4.0% to approximately 0.1%. As a result, there is no need to measure the salt density at 500 °C for inventory operations; the model for the salt density is found to be accurate.

1. Introduction

Idaho National Laboratory is conducting the treatment of spent metallic fuel, which began as a demonstration program by Argonne National Laboratory in 1996 [1–3]. In the key step, the metal fuel is electrorefined in a molten LiCl–KCl electrolyte. At startup of the electrorefiner [4,5], the molten LiCl–KCl eutectic salt was charged with UCl_3 to a nominal concentration of 6 wt.% U^{+3} (8.7 wt.% UCl_3) to support the electrorefining process. As uranium metal electrochemically dissolves from the spent fuel into the salt as U^{+3}, purified uranium metal electrochemically deposits out of the salt onto the cathode.

When the inventory of U^{+3} was determined from time to time, two measurements and one calculation were performed [6]. First, the depth of the molten salt layer was measured to determine the volume of molten salt, since the volume had been calibrated with the liquid depth in separate procedures. Second, the weight fraction of U^{+3} in salt samples was measured using mass spectrometry on salt samples. Third, the salt density was calculated using additive volumes, so that the product of the three values computed as the mass of U^{+3} dissolved in the salt.

The density of molten eutectic LiCl–KCl can be calculated to great accuracy using the individual salt densities because the solution exhibits ideal behavior ($\Delta H_{mix} = 0$)[1] [7]. Regression of Van Artsdalen and Yaffe's data and supercooling the densities gives exceptional agreement between the measured eutectic density and calculated density by additive volumes [7]. Ideal solution behavior indicates that repulsive interactions and attractive interactions are negligible. This may be expected in that the coordination sphere of Li^+ and K^+ in the Cl^- environment would be comparable; the Cl^- ion would bond approximately equally (and weakly) toward either cation in the melt. On the other hand, the chloride ion would be expected to be bonded more strongly to U^{+3} because of the higher charge density in comparison to Li^+ or K^+, and should be reasonably expected to form a complex, such as the UCl_6^{-3} ion [8,9].

The chemical interaction producing the UCl_6^{-3} complex renders the molten salt solution non-ideal with respect to the U^{+3} ion. It indicates a negative enthalpy of mixing, because of the attractive interaction. As a consequence, the calculated density will not be accurate by reason of the bias introduced with dissolved U^{+3}. Furthermore, the concentrations of lanthanide (which are mostly trivalent cations) and alkaline earth (divalent cations) ions grow into the salt phase as more spent fuel is treated. The bias then is not constant but increases with the treatment of each batch of fuel. The salt density therefore needs to be analyzed and modeled, as reported in this paper.

Abbreviations: REBUS/RCT-3, a nuclear reactor fuel cycle/depletion code; ASME, American Society of Mechanical Engineers.

* Corresponding author. Tel.: +1 (208) 533 7609; fax: +1 (208) 533 7471.
E-mail address: DeeEarl.Vaden@inl.gov (D. Vaden).

[1] If $\Delta H_{mix} = 0$, then $\Delta(PV)_{mix} = [V\Delta P + P\Delta V]_{mix} = 0$. Therefore, at constant pressure, $\Delta V_{mix} = 0$.

0022-3115/$ - see front matter © 2010 Elsevier B.V. All rights reserved.
doi:10.1016/j.jnucmat.2010.06.022

2. Background

The two types of fuel being treated are driver fuel and blanket fuel. These two types of fuel were treated in two different electrorefiners with different batch sizes and different hardware. The electrorefiner treating driver fuel is shown in Fig. 1. While the modeling of the molten salt density and the calculation of the salt mass follow the same arguments regardless of fuel type, the driver fuel contains more lanthanides and more quickly influences the salt density. Only the driver fuel will be discussed here. A brief summary of the process is given below, and the interested reader can consult other articles for more detail [10–13].

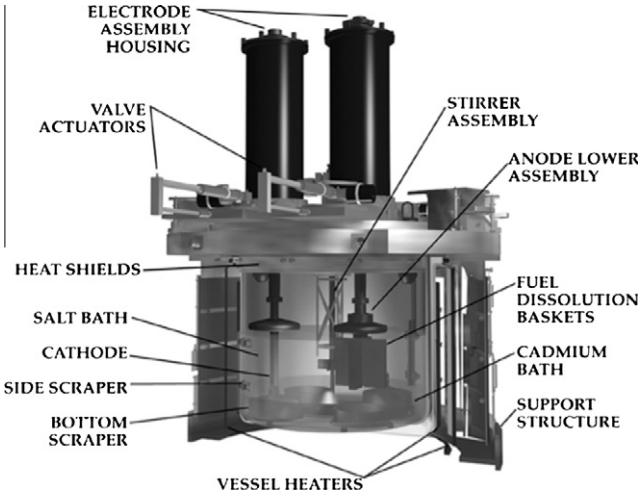

Fig. 1. Mark IV electrorefiner.

The electrorefiner vessel, constructed of 2¼Cr–1Mo alloy steel (ASME Spec. SA-387Gr22), had a 101.6 cm diameter and contained a nominal fluid depth of 45.7 cm. The LiCl–KCl molten salt depth was nominally 30.5 cm and rested on top of a Cd pool layer with a depth on the order of 15.2 cm. The salt depth was measured using a resistance-based probe, which detected the gas–salt interface (top of the salt) and salt–cadmium interface (bottom of the salt).

Perforated steel baskets were used to contain the chopped spent fuel for electrorefining, as shown in Fig. 2. A sample composition of the chopped fuel is provided in Table 1. The composition is modeled with a validated code, REBUS/RCT-3 [14]. On occasion, chopped fuel pin samples were selected from prescribed positions on the fuel column to confirm the modeled data.

After the steel baskets with chopped fuel were immersed in the molten salt, they were connected as the anode to the power supply. A steel mandrel was connected as the cathode and refined uranium was collected on the mandrel as a dendritic mass with adhering salt, as shown in Fig. 3. The adhering salt was returned to the electrorefiner after a separate vacuum distillation operation that also consolidated dendrites into a uranium ingot.

It was desirable to hold the U^{+3} concentration fairly constant to support a reasonable and consistent electrorefining rate (U^{+3} must be supplied to the cathode surface as soon as the power supply is

Table 1
Typical composition of irradiated driver fuel.

Element	wt.%	Element	wt.%	Element	wt.%
U	85.34	La	0.22	Pm	0.023
Zr	11.00	Pr	0.21	Fe	0.010
Nd	0.71	Sm	0.12	Cd	0.005
Ce	0.42	I	0.04	Br	0.005
Pu	0.30	Np	0.03	Ag	0.003

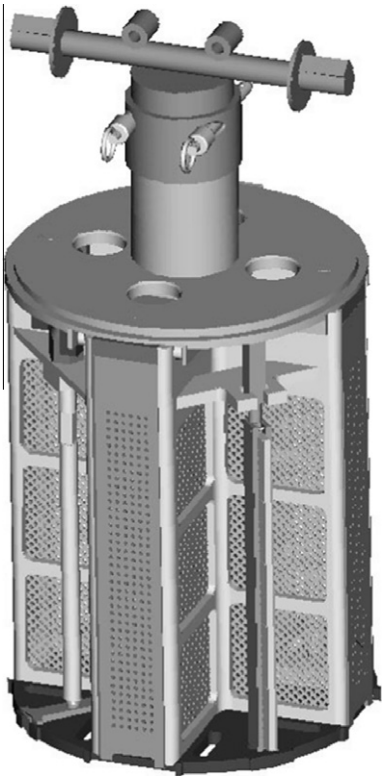

Fig. 2. Perforated driver fuel dissolution baskets.

Fig. 3. Dendritic uranium deposit.

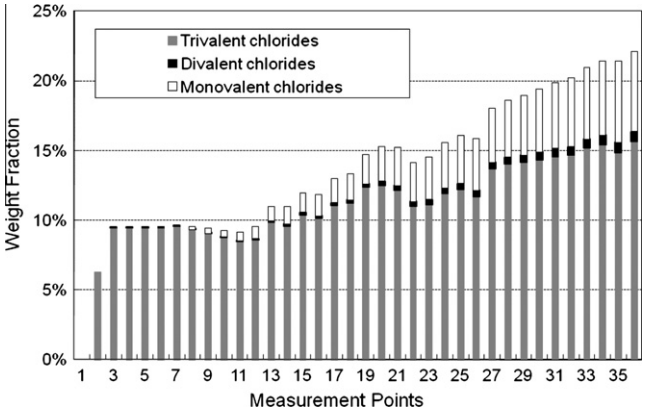

Fig. 4. In-growth of fission product chlorides in the molten salt.

actuated to support the current or other salt components would be reduced). However, prior to passing current, when the chopped fuel was initially immersed in the molten salt, oxidation–reduction reactions occurred between the U^{+3} present in the molten salt and spent fuel components [15]. The more active metals in the spent fuel would be oxidized to form dissolved chlorides as they reduced the dissolved U^{+3} [16], as in:

$$Nd_{fuel} + U^{+3}_{salt} \rightarrow Nd^{+3}_{salt} + U_{on\ cladding} \quad (1)$$

To recover the U^{+3} content and maintain a nominally steady state concentration, occasional additions of $CdCl_2$ were made at a time when the cadmium pool was laden with dissolved uranium metal:

$$2\,U_{Cd\ pool} + 3\,CdCl_2 \rightarrow 3\,Cd_{Cd\ pool} + 2\,UCl_3 \quad (2)$$

It is important to note that the lanthanide concentration in the salt therefore increases with each batch of fuel, and that the weight fraction of trivalent cations in the salt (actinides plus lanthanides) increases. As more fuel is treated and the trivalent cation content increases, as shown in Fig. 4, any non-ideal solution behavior will worsen. In Fig. 4, the balance of the salt mass (up to 100% weight fraction) is made up by the LiCl–KCl eutectic, so that the first measurement corresponds to the presence of eutectic only. UCl_3 was charged to the salt for the second measurement point. Irradiated fuel was introduced prior to the ninth measurement point, thereby introducing fission product chlorides such as CsCl, $SrCl_2$, and $NdCl_3$ as well as NaCl from the bond sodium. This change over time is what raises the concern over inaccuracies in the calculated salt density and heavy metal inventory.

3. Material and methods

The electrorefiner (ER) salt volume (V) was determined from measuring the salt depth because a correlation between the two was established during two independent volume calibrations [17]. Since the mass (M) of LiCl–KCl eutectic was taken before each addition, the mass and volume of eutectic salt resulted in a measured salt density (ρ) for the molten eutectic:

$$\rho_{LiCl-KCl,\ measured} = \frac{M_{LiCl-KCl\ in\ ER,\ measured}}{V_{salt\ in\ ER,\ measured}} \quad (3)$$

The salt density for the molten eutectic could also be calculated using the principle of additive volumes because the weight fractions (w) of the components were known and the solution is ideal:

$$\frac{1}{\rho_{eutectic,\ calculated}} = \frac{w_{LiCl}}{\rho_{LiCl,\ 500\ ^\circ C}} + \frac{w_{KCl}}{\rho_{KCl,\ 500\ ^\circ C}} \quad (4)$$

The densities used in Eq. (4) are the supercooled densities of the pure components.

Since the ER was operated at two temperatures and the literature data was extensive [7], an experimental regression of the data was preferred, as in:

$$\rho_{literature}\ (g/mL) = \begin{array}{c} 1.954695 - 0.177580 \cdot w_{LiCl} - 0.000559 \cdot t\ (^\circ C) \\ + 0.000110 \cdot w_{LiCl} * t\ (^\circ C) \end{array} \quad (5)$$

A comparison of the three eutectic salt densities ($\rho_{measured}$, $\rho_{calculated}$, $\rho_{literature}$) gave excellent agreement (within 1% or less), demonstrating ideal solution behavior.

After UCl_3 was introduced to the molten salt, the measured salt density continued to be determined using the net measured salt masses and measured salt volume and Eq. (3). On the other hand, the salt density could be calculated assuming ideal solution behavior:

$$\frac{1}{\rho_{salt,\ calculated}} = \frac{w_{LiCl}}{\rho_{LiCl,\ 500\ ^\circ C}} + \frac{w_{KCl}}{\rho_{KCl,\ 500\ ^\circ C}} + \frac{w_{UCl_3}}{\rho_{UCl_3,\ 500\ ^\circ C}} \quad (6)$$

However, the calculated density was thought to give a detectable bias because the U^{+3} concentration was more than dilute (6 wt.% U^{+3}) and because the coordination chemistry of the chloride ion toward U^{+3} would not give ideal solution behavior. A comparison of measured and calculated densities was made, and a bias was in fact observed and further detailed in the discussion.

The heavy metal inventory is determined from the salt chemical analysis (e.g., wt.% U^{+3}), measured salt volume, and the density of the salt:

$$M_{U,measured} = \rho_{salt} \cdot V_{salt} \cdot \frac{wt.\%\ U_{measured}}{100} \quad (7)$$

As spent fuel was treated in the ER the salt composition content varied with the accumulation of lanthanide, alkaline earth, and alkali metal chlorides (see Fig. 4). As the above equations indicate, the calculation of the salt density requires another term for each salt component. The assumption of ideal solution behavior became more suspect. In order to determine salt density, it became necessary to either measure both salt composition and density separately, or measure the salt composition and model the salt density.

The latter course was adopted for the following reasons. First, a variety of errors are possible and difficult to control during repetitive determinations of the density of hygroscopic salt samples at 500 °C in a hot cell environment. Second, considerable success was observed with the calculated salt density, and it was believed a reliable model could be developed. Third, it was more economical to model the salt density. Last, the possibility of measuring the salt density at 500 °C for select samples was held in reserve in the event it was discovered to be necessary.

Table 2
Salt density evaluation.

Method	Behavior	Application
Measured	As accurate and precise as the measurement methods	Net mass of salt in the ER (determined from weights) divided by the salt volume (determined from ER volume calibration)
Calculated	Ideal solution behavior. Uses method of additive volumes	Eutectic LiCl–KCl with no bias. Eutectic LiCl–KCl–8.7%UCl_3 with a constant bias expected for a constant UCl_3 content
Modeled	Accuracy and precision to be developed and demonstrated with spent fuel treatment	Measured and modeled salt composition used to assess bias present for trivalent cations with a limited data set. Extended data set used to confirm model validity

While measuring the salt composition appears useful and straightforward, it is economically prohibitive to measure every salt component because so many components are introduced by the spent fuel. Even if every component were measured, experimental error in the analyses guarantees the components will not add to 100.0% and subsequently, the mass will not be conserved. An algorithm is therefore required at least to perform the normalization, and since some analyses have less error than others, the composition must also be modeled. However, as will be seen in this discussion, the chemical analyses for some of the cations are preserved in the algorithm: e.g., a salt sample analysis reporting 6.00 wt.% U^{+3} is always preserved by the algorithm as exactly 6.00 wt.% U^{+3} in the modeled composition.

In summary, the modeled salt density (ρ_{model}) was expected to be different from the calculated salt density ($\rho_{calculated}$),[2] as provided in Table 2. The reasons a difference was expected and modeling is required are that (1) the chloride coordination in the melt is stronger for trivalent cations than monovalent cations, and (2) the trivalent cation content of the molten salt grows in as more spent fuel is treated, rendering the heavy metal inventory operations for the molten salt problematic.

The modeled salt density (ρ_{model}) was expected to be different from the measured salt density ($\rho_{measured}$). This difference could be assessed and was first applied to develop an algorithm for modeling the salt density with a limited data set early in the spent fuel treatment. After the algorithm was developed, the small difference between ρ_{model} and $\rho_{measured}$ confirmed the model validity by demonstrating the average bias was zero or negligible with an extended data set.

Table 3
Molten salt densities for pure components germane to electrorefining spent metallic fuel. The composition corresponds to having treated 50 irradiated fuel assemblies (205 kg heavy metal).

Metal chloride	*A*	*B*	*C*	g/ml @ 500 °C	In electrolyte (wt.%)
KCl	2.1359	−5.831E-04	273.15	1.6851	42.54
LiCl	1.8842	−4.328E-04	273.15	1.5496	35.23
UCl_3	6.3747	−1.522E-03	273.15	5.1980	11.69
NaCl	2.1393	−5.430E-04	273.15	1.7195	4.87
$NdCl_3$	**5.0659**	**−1.522E-03**	273.15	3.8891	1.34
$CeCl_3$	4.2480	9.200E-04	273.15	4.9593	0.81
CsCl	3.7692	−1.065E-03	273.15	2.9458	0.80
$PuCl_3$	**6.6252**	**−1.522E-03**	273.15	5.4485	0.47
$LaCl_3$	4.0895	7.774E-04	273.15	4.6905	0.42
$PrCl_3$	**4.9624**	**−1.522E-03**	273.15	3.7855	0.39
$BaCl_2$	4.0152	6.813E-04	273.15	4.5419	0.38
$SrCl_2$	3.3896	5.781E-04	273.15	3.8366	0.33
YCl_3	3.0070	5.000E-04	273.15	3.3936	0.22
$SmCl_3$	**5.3767**	**−1.522E-03**	273.15	4.1998	0.20
RbCl	3.1210	−8.832E-04	273.15	2.4382	0.11
$NpCl_3$	**6.4314**	**−1.522E-03**	273.15	5.2545	0.04
$PmCl_3$	**5.4285**	**−1.522E-03**	273.15	4.2516	0.04
$EuCl_2$	**5.7910**	**−1.522E-03**	273.15	4.6141	0.01
$GdCl_3$	**5.4332**	**−1.522E-03**	273.15	4.2563	0.01
$MgCl_2$	1.9760	3.020E-04	273.15	2.2095	0.00
$TbCl_3$	**5.2731**	**−1.522E-03**	273.15	4.0962	0.00
$CaCl_2$	2.5261	4.225E-04	273.15	2.8528	0.00
$AmCl_3$	**6.6197**	**−1.522E-03**	273.15	5.4428	0.00
$CmCl_3$	**6.6479**	**−1.522E-03**	273.15	5.4710	0.00
$CdCl_2$	4.0150	−6.813E-04	273.15	3.4883	0.00
$BeCl_2$	2.2760	−1.100E-03	273.15	1.4255	0.00
AgCl	5.4890	8.490E-04	273.15	6.1454	0.00

4. Application of the method and modeled salt density

In practice, the most direct evaluation of material balance can be made from the net weights. The net weights of chloride salts in the ER at various times are known directly from measured weights of materials added to or taken from the ER. The net weight gives directly a measured salt mass (M_{meas}) that can be compared to a modeled salt mass (M_{model}) as determined from:

$$M_{model} = V_{salt} \cdot \rho_{model} \tag{8}$$

where the salt volume (V_{salt}) is obtained from salt depth measurements correlated as part of the volume calibration.

It is the value of ρ that causes the discrepancy between the measured and modeled salt masses. While the salt consisted of LiCl–KCl eutectic only, the calculated density introduced no perceptible error in the salt mass. Upon introducing UCl_3, a small error resulted because the modeled density is not the true density. Upon processing spent fuel, the error propagated with increasing trivalent chloride content because of the bias in the modeled density for the trivalent chlorides. In the discussion that follows, the measured and modeled masses will be used to give the direct comparison needed for detecting the error and guiding the development of the salt density model.

In a multi-component ideal solution, the calculated density is:

$$\frac{1}{\rho_{calculated}} = \sum \left(\frac{w_i}{\rho_i}\right) \tag{9}$$

The densities for pure salts involved in the electrorefining process are listed in Table 3, along with their temperature dependence. For the ideal solution, these densities at 500 °C are used to calculate the total mass of salt in the electrorefiner. They form the reference point for evaluating inventory difference. If the total salt mass is in error, the analyzed weight fraction of uranium in the salt will propagate the error when computing the salt inventory, regardless of the accuracy for the sampling and analysis events.

Table 3 also contains the constants used to determine the densities of the metal chlorides as a function of temperature via Eq. (10), where ρ is the density of the metal chloride in g/cc and t is the temperature in Celsius:

$$\rho = A + B \cdot (C + t) \tag{10}$$

All data in Table 3 are taken from Janz [18], except UCl_3 [19], and the metal trichlorides in bold, which were calculated. Data for the lanthanide and actinide chlorides (e.g., $PuCl_3$) at 500 °C was not found in the literature. Their densities were estimated using the data for UCl_3 under the assumption that the volume expansion for the solid would be identical to that for UCl_3.

It was prohibitive to analyze every salt component for the purpose of calculating the salt density, making it necessary to model a portion of the salt composition. Even if all components were analyzed, their weight fractions would not sum to unity (i.e., 100%) because of experimental error. It was apparent that a normalization algorithm was needed to adjust the relative weight fractions, and modeling was necessary even if every salt component was analyzed.

After processing 100 Experimental Breeder Reactor-II driver assemblies, or 0.4 metric tons of heavy metal (HM), the modeled composition of the salt, in cumulative weight percent, is shown in Fig. 5. The normalization model that was adopted preserves the analytical results for the cations measured with high accuracy and precision (e.g., U^{+3} and Pu^{+3} at 0.5% relative analytical error [20]) and for as many measured cations in the LiCl–KCl salt as are possible.

First, the metal chloride weight fraction was calculated from the cation weight fraction via Eq. (11):

$$F_i = N_i \left[1 + z_i \frac{Mwt_{Cl}}{Mwt_i}\right] \tag{11}$$

[2] *Calculated salt density* is reserved to designate ideal solution behavior.

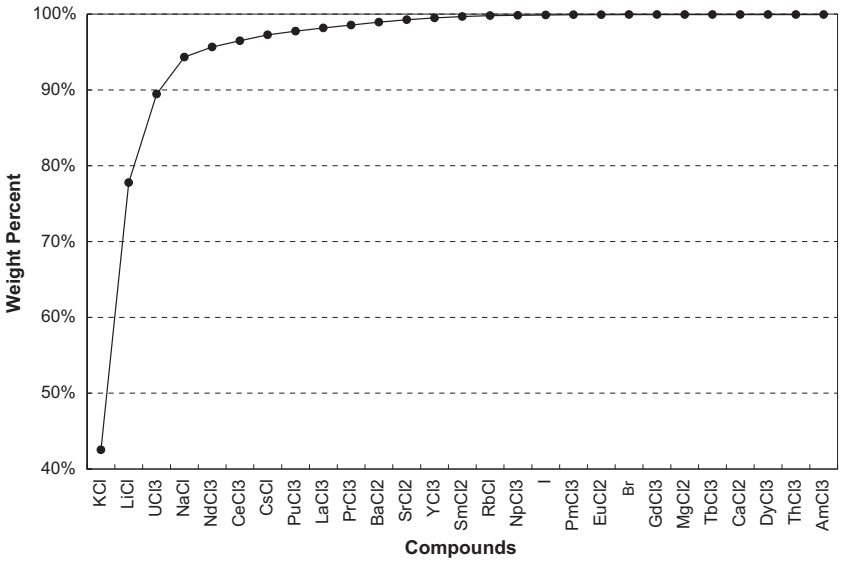

Fig. 5. Cumulative composition in Mark-IV ER salt after processing 100 driver assemblies.

where F_i is the metal chloride weight fraction, N_i is the element weight fraction, z_i is the charge of the metal ion, Mwt_{Cl} is the molecular weight of chlorine, and Mwt_i is the molecular weight of the metal component in the metal chloride. The remaining cations were then adjusted so that the weight fractions of the measured metal chlorides and the adjusted metal chlorides sum to unity, as shown in Eq. (12):

$$1 = \sum_i F_i^P + \sum_k F_k^P = \sum_i F_i^M + \sum_k F_k^A = \sum_i F_i^M + X\sum_k F_k^P$$
$$F_k^A = X \cdot F_k^P = \left[\frac{1-\sum_i F_i^M}{1-\sum_i F_i^P}\right] \cdot F_k^P \quad i \neq k \tag{12}$$

where F_k^A and F_k^P represent the adjusted and predicted weight fractions of the cations not measured, respectively. Subsequently, F_i^M and F_i^P represent the measured and predicted weight fractions of the measured cations, respectively. The X term is the adjustment factor, which is a function of the measured and predicted weight fractions.

Finally, the modeled ER salt density [ρ_{model}] is determined from the adjusted weight fractions [F_k^A] and measured weight fractions [F_i^M] of the metal chlorides along with their respective metal chloride densities [ρ_i and ρ_k] using additive volumes, as shown in Eq. (13):

$$\frac{1}{\rho_{model}} = \sum_k \frac{F_k^A}{\rho_k} + \sum_i \frac{F_i^M}{\rho_i} \tag{13}$$

After modeling the salt density with this equation, the modeled salt mass (M_{model}) was computed and compared to the measured salt mass (M_{meas}, the net mass of salt determined from weights). This comparison was used to detect any bias and to assess the accuracy of the modeled salt density, by inference. More importantly, the merit of any adjustments to the model for calculating the salt density calculation could be evaluated, as discussed.

5. Discussion

Salt density modeling proceeded in three stages. In the first stage, it was confirmed that a small bias was introduced upon introduction of depleted UCl_3, i.e., the measured and predicted salt masses differed, presumably from a small error in the calculated salt density. Further, the bias increased with increasing lanthanide content of the salt. In the second stage, a sensitivity analysis was performed on a limited set of data to examine the effects of correcting for trivalent cations, divalent cations, and monovalent cations. In the third stage, the adequacy of the correction factors was tested by continuing to apply the correction factors to a much larger set of data. Of course, it was necessary to assume that no process losses occurred in the salt phase (such as conversion to oxide from impurities) during the time span for data collection.

5.1. Stage one

In Fig. 6, the mass balance determinations for 26 events are displayed. The first data point represents the addition of the LiCl–KCl salt initially loaded into the ER. The next seven data points represent mass balance events for depleted uranium (DU) operations only. Subsequent data points indicate operations with chopped spent fuel, the introduction of lanthanides, and the need to adjust the UCl_3 concentration. The last measurement point corresponds to having processed a total of 205 kg HM from spent fuel. The average percent difference for this data set is 4.39% ± 5.74%, indicating a strong bias. More importantly, the percent difference and its standard deviation become greater after the introduction of the spent fuel as expected (see bold area of Table 4).

5.2. Stage two

After confirming a bias was present with the accumulation of multi-valent cations, stage two focused on finding the factor k in the density equation $\rho = kA + B(C + t)$ to reduce the average percent difference between the measured salt mass and the predicted salt mass. A k factor of unity implies an ideal solution. For example, reducing the percent difference for the initial salt loading to zero required a k factor of 0.99973. This verifies that the LiCl–KCl salt is an ideal solution near the eutectic composition. Since the initial LiCl–KCl salt is composed of monovalent metal chlorides, it was assumed that all monovalent metal chlorides (e.g., Na, Cs) also behave ideally.

Table 4 shows the metal chloride weight fraction of monovalent, bivalent, and trivalent chlorides accumulating in the salt after processing DU and 205 kg HM of spent fuel. Less than 0.5% of the metal chlorides forming in the salt from processing spent nuclear fuel are divalent chlorides. Assuming the monovalent chlorides

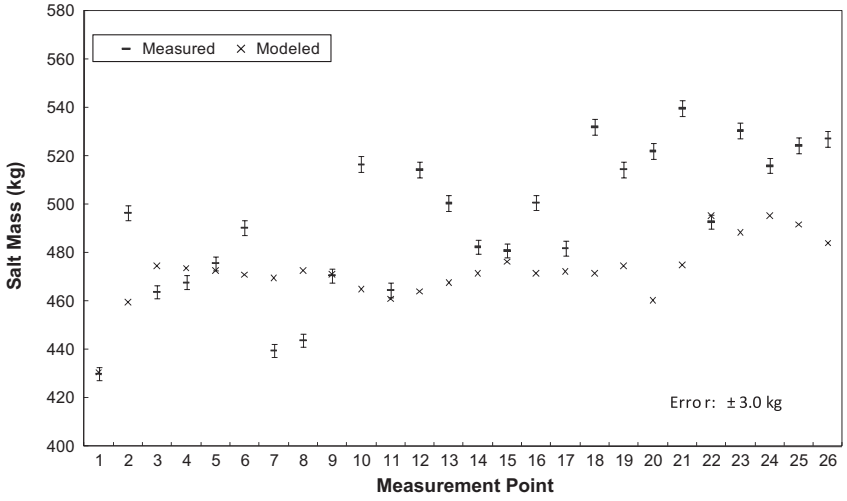

Fig. 6. Measured and modeled salt masses where the modeled salt mass applies additive volumes.

Table 4
Percent differences between measured and predicted salt mass at stage three.

	Stage 1	Stage 2	Stage 3
	Average ± 1σ	Average ± 1σ	Average ± 1σ
LiCl–KCl	**−0.14%**[a]	0.00%[a]	0.00%[a]
After DU tests	**−0.41% ± 4.86%**	0.00% ± 0.33%	−0.37% ± 0.37%
After DU and 99 kg HM	**2.23% ± 5.14%**	0.22% ± 0.70%	−0.21% ± 0.67%
After DU and 205 kg HM	**4.39% ± 5.74%**	0.53% ± 0.78%	0.00% ± 0.69%
After DU and 254 kg HM	4.29% ± 5.40%	0.72% ± 1.00%	0.12% ± 0.90%
After DU and 311 kg HM	5.24% ± 5.66%	0.58% ± 1.09%	−0.09% ± 1.07%

[a] Only one data point.

behave ideally and noting the bivalent chlorides constitute a small fraction, the focus switched to the trivalent chlorides, especially UCl_3, which is the majority of the trivalent chlorides and the only trivalent chloride at the end of DU operations. At measurement point number eight, the average percent difference was 0.73% ± 0.43%. This marked the beginning of the bias noted previously. Adding uranium to the salt, which forms a trivalent metal chloride, increased the percent difference from 0.03% (initial ER loading of LiCl and KCl) to an average of 0.73% ± 0.43% (UCl_3 additions). Attention was thus directed toward the UCl_3 for non-ideal solution behavior and a k factor in the density equation $\rho = kA + B(C + t)$ for UCl_3.

Fig. 7 is the result of using $k = 0.99973$ for the monovalent chlorides and $k = 0.82601$ for uranium trichloride to minimize the average percent difference for the first eight measurement points. The average percent difference between the predicted and measured salt mass at this measurement point was 0.00% ± 0.33%. This result is much improved over previous results with no density adjustment.

5.3. Stage three

In the final stage of modeling that applied data for processing the irradiated fuel, attention was directed toward the actinide and lanthanide chlorides for non-ideal solution behavior. The trivalent lanthanide fission products are chemically similar to the actinides, insofar as the solution behavior in molten alkali chlorides and the crystal structure types of their trivalent chlorides are concerned [21]. The existence of the UCl_6^{-3} complex ion in molten alkali chlorides has been demonstrated [22]. These observations suggest that if deviations from ideal solution behavior can occur for UCl_3, deviations can occur for the other species as well. Their abundance also indicates deviations from ideal solution behavior

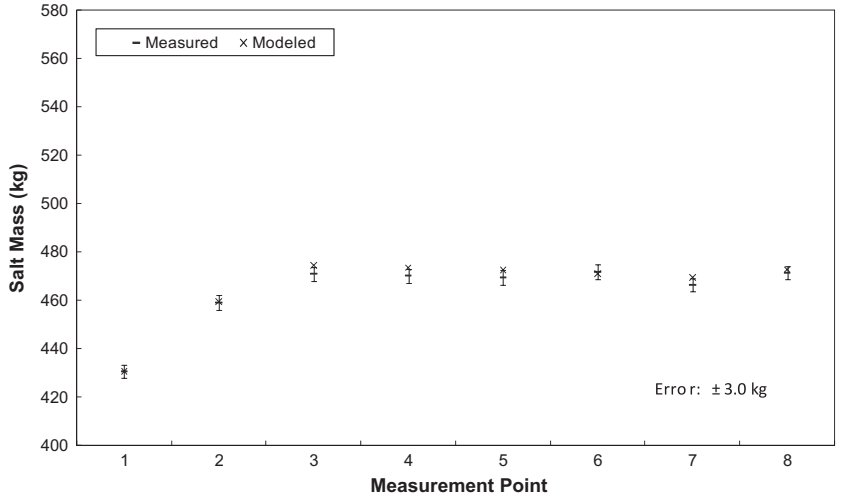

Fig. 7. Measured and modeled salt masses where the modeled salt mass applies a correction factor for U^{+3}.

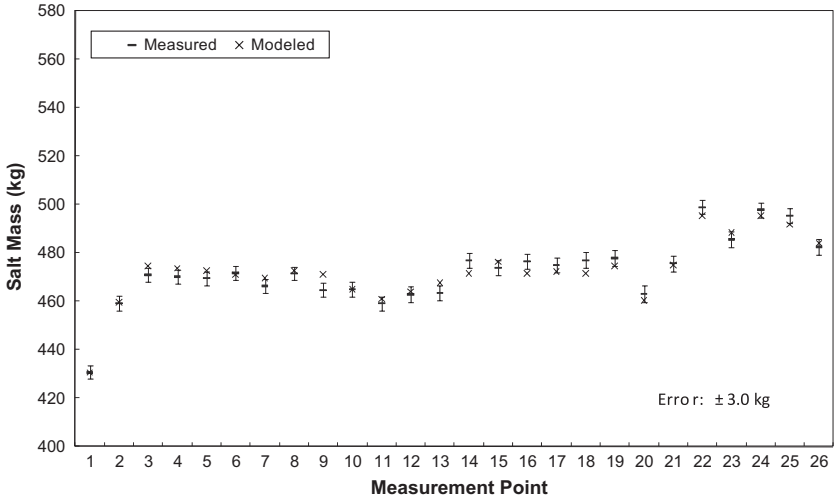

Fig. 8. Measured and modeled salt masses where the modeled salt mass applies a correction factor for all trivalent chlorides.

may be observable. Thus a solution was sought for the value of '*k*' in the density equation $\rho = kA + B(C + t)$ for the trivalent metal chlorides, including UCl_3.

Fig. 8 shows the result of using $k = 0.99973$ for the monovalent chlorides, $k = 0.99939$ for the divalent chlorides, and 0.76010 for the trivalent chlorides to minimize the average percent difference for the 26 measurement points. The average percent difference between the predicted and measured salt mass at this measurement point was 0.00% ± 0.69%. This result is much improved over previous results with no density adjustment. Table 4 lists the results of the density adjustment for further irradiated fuel processing.

6. Conclusion

It was found that the density of molten salt for treating spent nuclear fuel could be modeled with good accuracy. The resulting modeled salt mass was compared to the measured net salt mass in three stages to demonstrate the improvements of the model, which applied additive volumes for the different salt components, except for the trivalent chlorides. A correction factor for the trivalent chlorides was determined to be necessary by fitting a limited set of data involving spent fuel treatment. The correction factor and model were validated by applying the correction factor to an extensive set of data. The chemical basis for the correction factor is the known chloride coordination chemistry of U^{+3}.

The modeling algorithm also required conservation of mass. The weight fractions of the salt components reported in the chemical analyses do not sum to unity, except by coincidence. To normalize the component fractions, the weight fractions of LiCl and KCl were adjusted as required so that the component weight fractions summed to unity.

It was prohibitive to analyze for every component in the molten salt. All of the elements in the spent metallic fuel that became chloride salts were determined from thermodynamics. Some of the salt components were not chemically analyzed or their analyses had high uncertainty. Their corresponding weight fractions in the molten salt were determined based on the validated REBUS/RCT-3 code.

Adjusting the density of the trivalent chlorides reduced the systematic bias introduced upon charging the eutectic salt with UCl_3. Improved accountancy was readily observed for the total salt mass and inferred for the heavy metal chloride components. The resulting salt density model along with the correction factor for trivalent chlorides may now be applied with good accuracy when electrorefining metal fuels in eutectic LiCl–KCl. It appears there is no need to measure the salt density at 500 °C to determine the mass in the electrorefiner for material balances.

US department of energy disclaimer

Acknowledgements

The submitted manuscript has been authored by a contractor of the US Government under DOE Contract DE-AC07-05ID14517. Accordingly, the US Government retains a nonexclusive, royalty-free license to publish or reproduce the published form of this contribution, or allow others to do so, for US Government purposes.

References

[1] National Research Council, Electrometallurgical Techniques for DOE Spent Fuel Treatment: Final Report, National Academy Press, Washington DC, 2000.
[2] R. Benedict, M. Goff, G. Teske, T. Johnson, Nucl. Sci. Technol. 3 (Suppl.) (2002) 749–752.
[3] R.W. Benedict, C. Solbrig, B. Westphal, T.A. Johnson. S.X. Li, K. Marsden, K.M. Goff, Pyroprocessing progress at Idaho National Laboratory, American Nuclear Society Global 2007, Boise, ID, September 9–13, 2007.
[4] K.M. Goff, R.D. Mariani, N.L. Bonomo, Depleted uranium start-up of spent fuel treatment operations at Argonne National Laboratory – West, Trans. Am. Nucl. Soc. 73, San Francisco, CA, October 29–November 2, 1995.
[5] K.M. Goff, R.D. Mariani, D. Vaden, N.L. Bonomo, S.S. Cunningham, Fuel conditioning facility electrorefiner start-up results, in: Proceedings of DOE

Spent Nuclear Fuel and Fissile Material Management Conference, Reno, NV, June 16–20, 1996.
[6] D. Vaden, R.W. Benedict, K.M. Goff, R.W. Keyes, R.D. Mariani, R.G. Bucher, A.M. Yacout, Material accountancy in an electrometallurgical fuel conditioning facility, in: Proceedings of DOE Spent Nuclear Fuel and Fissile Material Management Conference, Reno, NV, June 16–20, 1996.
[7] E.R. Van Artsdalen, I.S. Yaffe, Electrical conductance and density of molten salt systems: KCl–LiCl, KCl–NaCl and KCl–KI, J. Phys. Chem. 59 (1955) 118–127.
[8] D.M. Gruen, R.L. McBeth, J. Inorg. Nucl. Chem. 9 (1959) 290–301.
[9] N.W. Silcox, H.M. Haendler, J. Phys. Chem. 64 (1960) 303–306.
[10] B.R. Westphal, R.D. Mariani, J. Miner. Metall. Mater. Simul. 52 (2000) 21–25.
[11] L. Burris, R. Steunenberg, W.E. Miller, The application of electrorefining for recovery and purification of fuel discharged from the integral fast reactor, AIChE Symposium Series No. 254, 83 (1987) 135.
[12] J.J. Laidler, J.E. Battles, W.E. Miller, J.P. Ackerman, E.L. Carls, Prog. Nucl. Energy 31 (1997) 131–140.
[13] J.P. Ackerman, Chemical Basis for Pyrochemical Reprocessing of Nuclear Fuel. I&EC Research, 29, 1991.
[14] R.D. McKnight, Validation of the REBUS-3/RCT methodologies for EBR-II core-follow analysis, in: Proceedings of Topical Meeting on Advances in Reactor Physics, 2, 69, Charleston, SC, March 8–11, 1992.
[15] J.P. Ackerman, I&EC Research 30 (1) (1991) 141.
[16] D.D. Keiser Jr., R.D. Mariani, J. Nucl. Mater. 270 (1999) 279–289.
[17] R.G. Bucher, Y. Orechwa, Fuel conditioning facility electrorefiner volume calibration, in: 36th Annual Meeting of the Institute of Nuclear Materials Management (INMM), Palm Desert, CA, July 9–12, 1995.
[18] G.J. Janz, Molten Salt Handbook, Academic Press, 1967.
[19] V.N. Desyatnik, S.F. Katyschev, S.P. Paspopin, Y.F. Chervinskii, Sov. Atom. Energy 39 (1975) 649–651.
[20] A.M. Yacout, et al. Nuclear material estimation and uncertainties for the spent fuel treatment at FCF, in: Proceedings of the Annual Meeting of the Institute of Nuclear Materials Management (INMM), Phoenix, AZ, July 25–29, 1999.
[21] A.W. Adamson, A Textbook of Physical Chemistry, Academic Press, 1973.
[22] L. Marinot, Molten-salt chemistry of actinides, in: A. J. Freeman, C. Keller (Eds.), Handbook on the Physics & Chemistry of the Actinides, vol. 6, p. 261, 308.